Frequency domain modeling of quasielastic neutron scattering from hydrated protein powders: Application to free and inhibited human acetylcholinesterase

Melek Saouessi (iD), Judith Peters (iD), and Gerald R. Kneller (iD)

View Online   **Export Citation**   **CrossMark**

ARTICLES YOU MAY BE INTERESTED IN

Frequency domain modeling of quasielastic neutron scattering from hydrated protein powders: Application to free and inhibited human acetylcholinesterase Ⓕ Ⓢᴄɪ

View Online   Export Citation   CrossMark

Melek Saouessi,[1,2] Ⓘᴅ Judith Peters,[3,4] Ⓘᴅ and Gerald R. Kneller[1,2,a)] Ⓘᴅ

AFFILIATIONS

[1] Centre de Biophys. Moléculaire, CNRS and Université d'Orléans, Rue Charles Sadron, 45071 Orléans, France
[2] Synchrotron Soleil; L'Orme de Merisiers, 91192 Gif-sur-Yvette, France
[3] Institut Laue Langevin, 71 Avenue des Martyrs, 38042 Grenoble Cedex 9, France
[4] Univ. Grenoble Alpes, CNRS, Laboratoire Interdisciplinaire de Physique, F-38000 Grenoble, France

[a)] E-mail: gerald.kneller@cnrs.fr

ABSTRACT

This article reports on a frequency domain analysis of quasielastic neutron scattering spectra from free and Huperzine-A-inhibited human acetylcholinesterase, extending a recent time domain analysis of the same experimental data [M. Saouessi *et al.*, J. Chem. Phys. **150**, 161104 (2019)]. An important technical point here is the construction of a semianalytical model for the resolution-broadened dynamic structure factor that can be fitted to the experimental spectra. We find comparable parameters as in our previous study and demonstrate that our model is sensitive to subpercent changes in the experimental data, which are caused by reversible binding of the inhibitor Huperzine A.

Published under license by AIP Publishing. https://doi.org/10.1063/1.5121703

I. INTRODUCTION

Quasielastic neutron scattering (QENS) is a powerful technique to explore the diffusive motions of atoms in condensed matter systems on nanometric length scales and (sub)nanosecond time scales.[1,2] Because of the dominant cross section of incoherent scattering from hydrogen, QENS studies of hydrogen-rich systems explore, in particular, the diffusive motions of individual hydrogen atoms and have been abundantly used to study the dynamics of biomolecular systems.[3,4] One challenge here is to reveal small changes in the internal functional dynamics of proteins as a result of external stress, such as hydrostatic pressure[5] or ligand binding.[6] A well-known difficulty in this context is the fusion of the elastic line with the quasielastic spectrum for systems in which global protein motions are suppressed, and it has been recently shown that this fusion can be explained by the self-similar slow relaxation dynamics of proteins.[7] In a recent analysis of QENS

data from free and Huperzine A (HupA)-inhibited Human Acetylcholinesterase (hAChE),[8] this aspect was taken into account by using a minimalistic three-parameter model in which the elastic intensity is fitted together with the parameters describing the relaxation dynamics. To remove the influence of the instrumental resolution, the data analysis was performed in the time domain, using a numerical Fourier transform of the sample and vanadium spectra, where the latter are used to estimate the instrumental resolution. Our analysis revealed quite subtle but systematic changes in the dynamics of hAChE upon inhibition through noncovalently bound HupA. These changes can be resumed in an average increase of the motional amplitudes of the hydrogen atoms and a slight slowing down of the relaxation dynamics of hAChE. We explained this effect within Frauenfelder's "energy landscape picture" by an increase of the barrier heights separating the multiple minima in the "rough" potential surface for the scattering hydrogen atoms.[9,10]

The main objective of this paper is to consolidate our previous study through a direct frequency domain analysis of the resolution-broadened experimental spectra, avoiding the numerical Fourier transform from the frequency to the time domain and the accompanying aliasing errors.

This paper is organized as follows: In Sec. II, we briefly present our analytical model for protein dynamics, and Sec. III contains the core of the paper—a description of a semianalytical method to fit the resolution-broadened model directly to the experimental QENS spectra. The direct analysis of QENS spectra of free and HupA-inhibited hAChE with our method is described in Sec. IV, and the paper is concluded by a short Résumé.

II. THEORY

A. General form of the scattering functions

The central observable in neutron scattering experiments is the dynamic structure factor. It carries information about the structure and dynamics of the scattering system,

$$S(\mathbf{q}, \omega) = \frac{1}{2\pi} \int_{-\infty}^{+\infty} dt\, e^{-i\omega t} F(\mathbf{q}, t), \qquad (1)$$

where $\mathbf{q}$ and ω denote the momentum and energy transfer from the neutron to the sample in units of $\hbar$, respectively. In experiments on hydrated protein powders, which will be analyzed in the following, incoherent scattering from the hydrogen atoms dominates and the intermediate scattering function, $F(\mathbf{q}, t)$, can be approximated by

$$F(\mathbf{q}, t) \approx \frac{1}{N_H} \sum_{\alpha \in H} \left\langle e^{-i\mathbf{q}\cdot\hat{\mathbf{x}}_\alpha(0)} e^{i\mathbf{q}\cdot\hat{\mathbf{x}}_\alpha(t)} \right\rangle, \qquad (2)$$

where $\hat{\mathbf{x}}_\alpha(t)$ are the position operators of the hydrogen atoms and $\langle\cdots\rangle$ denotes a quantum ensemble average. It follows from the symmetry properties of quantum time correlation functions and from the requirement that $S(\mathbf{q}, \omega)$ must be real that $F(\mathbf{q}, t)$ and $S(\mathbf{q}, \omega)$ fulfill the detailed balance relations

$$F(\mathbf{q}, -t) = F(\mathbf{q}, t + i\beta\hbar), \qquad (3)$$
$$S(\mathbf{q}, -\omega) = S(\mathbf{q}, \omega) \exp(-\beta\hbar\omega). \qquad (4)$$

Here, $\beta = 1/(k_B T)$, where k_B is the Boltzmann constant and T is the temperature in Kelvin. Equation (4) expresses that neutron energy gain is less likely than neutron energy loss.

In hydrated powder samples, where rigid-body motions of whole proteins are suppressed and the motional amplitudes of individual hydrogen atoms are finite, the intermediate scattering function tends for large times to a finite plateau value,

$$\lim_{t\to\infty} F(\mathbf{q}, t) = \sum_{\alpha \in H} \left| \left\langle e^{i\mathbf{q}\cdot\hat{\mathbf{x}}_\alpha} \right\rangle \right|^2 \equiv EISF(\mathbf{q}), \qquad (5)$$

which is referred to as the Elastic Incoherent Structure Factor (EISF). Defining

$$\delta\hat{\rho}_\alpha(\mathbf{q}, t) = e^{i\mathbf{q}\cdot\hat{\mathbf{x}}_\alpha(t)} - \left\langle e^{i\mathbf{q}\cdot\hat{\mathbf{x}}_\alpha} \right\rangle \qquad (6)$$

to be the deviation of the spatially Fourier transformed single particle density of atom α with respect to its mean value and $\phi(\mathbf{q}, t)$ to be the corresponding atom-averaged normalized autocorrelation function,

$$\phi(\mathbf{q}, t) = \frac{1}{N_H} \sum_{\alpha \in H} \frac{\left\langle \delta\hat{\rho}_\alpha^\dagger(\mathbf{q}, 0)\delta\hat{\rho}_\alpha(\mathbf{q}, t) \right\rangle}{\left\langle \delta\hat{\rho}_\alpha^\dagger(\mathbf{q}, 0)\delta\hat{\rho}_\alpha(\mathbf{q}, 0) \right\rangle}, \qquad (7)$$

the intermediate scattering function may be written in the generic form

$$F(\mathbf{q}, t) = EISF(\mathbf{q}) + (1 - EISF(\mathbf{q}))\phi(\mathbf{q}, t). \qquad (8)$$

For the dynamic structure factor, this translates into

$$S(\mathbf{q}, \omega) = EISF(\mathbf{q})\delta(\omega) + (1 - EISF(\mathbf{q}))\tilde{\phi}(\mathbf{q}, \omega), \qquad (9)$$

where $\delta(\omega)$ is the Dirac delta distribution and

$$\tilde{\phi}(\mathbf{q}, \omega) = \frac{1}{2\pi} \int_{-\infty}^{+\infty} dt\, e^{-i\omega t} \phi(\mathbf{q}, t) \qquad (10)$$

is the Fourier transformed relaxation function.

B. Semiclassical approximation

As in our previous analysis,[8] we will be using the normalized "shifted" relaxation function

$$\phi^{(+)}(\mathbf{q}, t) = \frac{\phi(\mathbf{q}, t + i\beta\hbar/2)}{\phi(\mathbf{q}, i\beta\hbar/2)}, \qquad (11)$$

which is real and symmetric in time. In frequency space, Relation (11) reads

$$\tilde{\phi}^{(+)}(\mathbf{q}, \omega) \propto e^{-\beta\hbar\omega/2}\tilde{\phi}(\mathbf{q}, \omega), \qquad (12)$$

noting that by construction

$$\int_{-\infty}^{+\infty} d\omega\, \tilde{\phi}^{(+)}(\mathbf{q}, \omega) = \phi^{(+)}(\mathbf{q}, 0) = 1. \qquad (13)$$

According to Eq. (8), we define the normalized symmetrized intermediate scattering function,

$$F^{(+)}(\mathbf{q}, t) = EISF(\mathbf{q}) + (1 - EISF(\mathbf{q}))\phi^{(+)}(\mathbf{q}, t), \qquad (14)$$

and the corresponding real and symmetric dynamic structure factor,

$$S^{(+)}(\mathbf{q}, \omega) = EISF(\mathbf{q})\delta(\omega) + (1 - EISF(\mathbf{q}))\tilde{\phi}^{(+)}(\mathbf{q}, \omega), \qquad (15)$$

which are by definition normalized,

$$\int_{-\infty}^{+\infty} d\omega\, S^{(+)}(\mathbf{q}, \omega) = F^{(+)}(\mathbf{q}, 0) = 1. \qquad (16)$$

The choice of working with $\phi^{(+)}(\mathbf{q}, t)$ and $\tilde{\phi}^{(+)}(\mathbf{q}, \omega)$ rather than with $\phi(\mathbf{q}, t)$ and $\tilde{\phi}(\mathbf{q}, \omega)$ is motivated by Schofield's semiclassical correction,[11] which consists in identifying the shifted relaxation function $\phi^{(+)}(\mathbf{q}, t)$ with its classical counterpart,

$$\phi^{(+)}(\mathbf{q}, t) \approx \phi^{(cl)}(\mathbf{q}, t). \qquad (17)$$

The Schofield correction is corrected up to first order in $\hbar$ and allows for using classical diffusion models to interpret QENS data from

complex systems, which have an essentially continuous energy spectrum. The correction requires $\beta\hbar\omega \ll 1$ as well as $\hbar^2 q^2/2m_{\text{eff}} \ll 1$, where m_{eff} is the effective mass of the scattering atom.

C. Minimal model for internal protein dynamics

In order to account for self-similar relaxation dynamics in proteins, we use the semiclassical approximation (17), where the classical correlation function is given by a stretched Mittag-Leffler function,[8]

$$\phi^{(+)}(t) = E_{\alpha,1}(-t^\alpha) \quad (0 < \alpha \le 1). \tag{18}$$

Here, the **q**-dependence is omitted and we use a dimensionless time scale to keep the notation concise. The (generalized) Mittag-Leffler function $E_{\alpha,\beta}(z)$ is an entire function in the complex plane,[12,13]

$$E_{\alpha,\beta}(z) = \sum_{k=0}^{\infty} \frac{z^k}{\Gamma(\beta + \alpha k)}, \tag{19}$$

which contains the exponential function as a special case, $E_{1,1}(z) = \exp(z)$. Here, $\Gamma(z)$ is the Gamma function or a generalized factorial.[13] In contrast to the model relaxation function defined in Eq. (18), its Fourier spectrum has a simple analytical form,

$$\tilde{\phi}^{(+)}(\omega) = L_\alpha(\omega), \tag{20}$$

where

$$L_\alpha(\omega) = \frac{\sin\left(\frac{\pi\alpha}{2}\right)}{\omega\left(\omega^{-\alpha} + \omega^\alpha + 2\cos\left(\frac{\pi\alpha}{2}\right)\right)} \tag{21}$$

can be considered as a "generalized Lorentzian function."

The self-similarity of the relaxation dynamics in proteins is accounted for by the scale-invariant power law form of the stretched Mittag-Leffler function for long times,

$$E_{\alpha,1}(-t^\alpha) \overset{t \gg 1}{\sim} \frac{t^{-\alpha}}{\Gamma(1 - \alpha)}, \tag{22}$$

which translates into a scale-invariant power law form

$$L_\alpha(\omega) \overset{\omega \ll 1}{\sim} \sin\left(\frac{\pi\alpha}{2}\right)\omega^{\alpha-1}, \tag{23}$$

for its Fourier spectrum at small frequencies. Note that the long time tail in Eq. (22) vanishes for $\alpha \to 1$, i.e., for exponential relaxation.

A physical model leading to a relaxation function of the form (18) is the fractional Ornstein-Uhlenbeck (fOU) process.[14] The normal Ornstein-Uhlenbeck process describes the diffusion of a Brownian particle in a harmonic potential[15] and the fractional generalization[16,17] includes non-Markovian memory effects resulting from the interactions of the diffusing particle with its environment. In our model, for the relaxation function, the position of the diffusing Brownian particle is replaced by the classical counterpart of the dynamical variable $\delta\rho_\alpha(\mathbf{q}, t)$, which is defined in Eq. (6), and the harmonic potential creates an elastic force driving $\delta\rho_\alpha(\mathbf{q}, t) \to 0$, or, equivalently, $\exp(i\mathbf{q} \cdot \mathbf{x}(t)) \to \langle\exp(i\mathbf{q} \cdot \mathbf{x})\rangle$. The resulting nonexponential relaxation function can be expressed as a superposition of exponential functions,
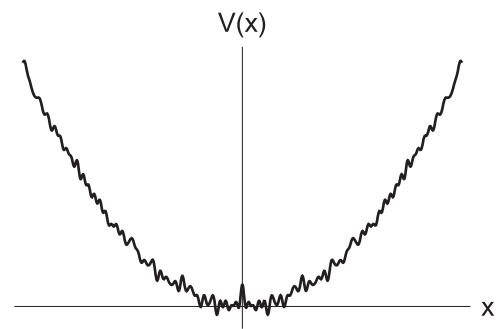

FIG. 1. Sketch of a rough harmonic potential.

$$E_{\alpha,1}(-t^\alpha) = \int_0^\infty p(\lambda) \exp(-\lambda t)\, d\lambda, \tag{24}$$

where $p(\lambda)$ is a continuous relaxation rate spectrum of the form

$$p(\lambda) = \frac{1}{\pi} \frac{\sin(\pi\alpha)}{\lambda(\lambda^\alpha + \lambda^{-\alpha} + 2\cos(\pi\alpha))}, \tag{25}$$

fulfilling $\int_0^\infty p(\lambda)\, d\lambda = 1$. We note that the moments $\overline{\lambda^n} = \int_0^\infty d\lambda\, \lambda^n p(\lambda)$ do not exist for $n \ge 1$.

The nonexponential relaxation can also be thought of as the result of the diffusion in a "rough" harmonic potential (see Fig. 1), where the roughness is defined by a distribution of energy barriers separating local minima. For this purpose, we use Zwanzig's theory of diffusion in rough potential,[9] which relates the diffusion constant D in a rough potential for a given energy barrier ΔE to its counterpart D_0 in the smooth envelope potential, $D = D_0 \exp(-[\beta\Delta E]^2)$. Using now that $D_0 \propto \lambda_0$ for diffusion in a harmonic potential, the relaxation rate spectrum given in Eq. (25) can be related to a spectrum of dimensionless energy barriers,

$$P(\epsilon) = \frac{1}{\pi} \frac{2\epsilon \sin(\pi\alpha)}{\exp(\alpha\epsilon^2) + \exp(-\alpha\epsilon^2) + 2\cos(\pi\alpha)}, \tag{26}$$

where $\epsilon = \beta\Delta E$.

III. INCLUDING INSTRUMENTAL RESOLUTION

A. Resolution-broadened QENS spectra

The model presented in Sec. II C describes the "ideal" dynamic structure factor and does not account for instrumental resolution. The experimentally observed dynamic structure factor is given by the convolution integral

$$S_R^{(+)}(\mathbf{q}, \omega) = (S^{(+)} * \tilde{R})(\mathbf{q}, \omega)$$

$$\equiv \int_{-\infty}^{+\infty} d\omega'\, S^{(+)}(\mathbf{q}, \omega - \omega')\tilde{R}(\mathbf{q}, \omega'), \tag{27}$$

where $\tilde{R}(\mathbf{q}, \omega)$ represents the **q**-dependent resolution function which is supposed to be even in ω. The latter is typically obtained

from a vanadium run or by recording the sample spectra at very low temperatures. Inserting the generic form (9) for the dynamic structure factor into Expression (27), one obtains the general expression

$$S_R^{(+)}(\mathbf{q}, \omega) = EISF(\mathbf{q})\tilde{R}(\mathbf{q}, \omega) + (1 - EISF(\mathbf{q}))\left(\tilde{\phi}^{(+)} * \tilde{R}\right)(\mathbf{q}, \omega) \tag{28}$$

for the experimentally observed dynamic structure factor, where the index "R" stands for "resolution-broadened." The challenge for the direct analysis of QENS experiments in the ω-domain is to construct an analytical expression for $S_R^{(+)}(\mathbf{q}, \omega)$ that can be fitted to experimental data. A corresponding method will be presented in Sec. III B.

B. Semianalytical convolution procedure

In the following, we will consider the convolution of two Fourier spectra, $\tilde{f}(\omega)$ and $\tilde{g}(\omega)$,

$$\tilde{h}(\omega) = (\tilde{f} * \tilde{g})(\omega), \tag{29}$$

where the Fourier transform pair $f(t) \leftrightarrow \tilde{f}(\omega)$ is defined through

$$\tilde{f}(\omega) = \frac{1}{2\pi} \int_{-\infty}^{+\infty} dt \, e^{-i\omega t} f(t), \tag{30}$$

$$f(t) = \int_{-\infty}^{+\infty} d\omega \, e^{i\omega t} \tilde{f}(\omega). \tag{31}$$

The convolution integral $\tilde{h}(\omega)$ may be expressed through the Laplace transform of $h(t)$,

$$\tilde{h}(\omega) = \frac{1}{\pi}\Re\left\{\hat{h}(i\omega)\right\}, \tag{32}$$

where $h(t) = f(t)g(t)$ on account of the convolution theorem of the Fourier transform,

$$\hat{h}(s) = \int_0^\infty dt \, e^{-st} f(t)g(t) \quad (\Re\{s\} > 0). \tag{33}$$

We suppose now that the Laplace transforms $\hat{f}(s)$ and $\hat{g}(s)$ are known, but not the Laplace transform of $h(t) = f(t)g(t)$. An approximation for the Laplace transform $\hat{h}(s)$ may be obtained by expressing $g(t)$ through the contour integral for the inverse Laplace transform,

$$g(t) = \frac{1}{2\pi i} \oint_C ds \, e^{st} \hat{g}(s), \tag{34}$$

and using a Padé-approximant,[13]

$$\hat{g}(s) \approx \frac{P(s)}{Q(s)}, \tag{35}$$

for its Laplace transform. Here, $P(s)$ and $Q(s)$ are polynomials of a given order in $s-s_0$, where s_0 is the reference point for the Padé-approximation in the complex s-plane. The essential point here is that the inverse Laplace transform of $\hat{g}(s)$ given by Eq. (35) can be

easily computed by means of the residue theorem and leads to a very simple expression

$$g(t) \approx \sum_k c_k e^{s_k t}, \tag{36}$$

where the coefficients c_k are given by

$$c_k = \lim_{s \to s_k}\left\{(s - s_k)\frac{P(s)}{Q(s)}\right\}. \tag{37}$$

We assume here for simplicity that all roots of $Q(s)$ have a multiplicity of 1.

With these prerequisites, the Laplace-transform $\hat{h}(s)$ is then approximated through

$$\begin{aligned}
\hat{h}(s) &\approx \int_0^{+\infty} dt \, e^{-st} f(t)\left\{\sum_k c_k e^{s_k t}\right\} \\
&= \sum_k c_k \int_0^\infty dt \, e^{-(s-s_k)t} f(t) \\
&= \sum_k c_k \hat{f}(s - s_k).
\end{aligned} \tag{38}$$

The approximation of $\hat{h}(s)$ is thus obtained by a weighted sum of shifted Laplace transforms $\hat{f}(s - s_k)$.

We illustrate the method for the autoconvolution of a normalized Gaussian function,

$$G_\sigma(\omega) = \frac{e^{-\frac{\omega^2}{2\sigma^2}}}{\sqrt{2\pi}\sigma},$$

the result of which is $(G_\sigma * G_\sigma)(\omega) = G_{\sqrt{2}\sigma}(\omega)$. In this case, we have $g(t) = \exp(-t^2\sigma^2/2)$, and the corresponding Laplace transform is given by

$$\hat{g}(s) = \frac{\sqrt{\frac{\pi}{2}}e^{\frac{s^2}{2\sigma^2}}\operatorname{erfc}\left(\frac{s}{\sqrt{2}\sigma}\right)}{\sigma},$$

where erfc denotes the complementary error function.[13]

Figure 2 shows the exact autoconvolution for $\sigma = 1$ (solid black line) compared to the approximation (dashed red line). The Padé approximation of $\hat{g}(s)$ has here been performed with $s_0 = 1$ and $m = n = 8$ for the orders of the polynomials $P(s)$ and $Q(s)$, respectively. We note that the absolute error is smaller than 1.2×10^{-6} for
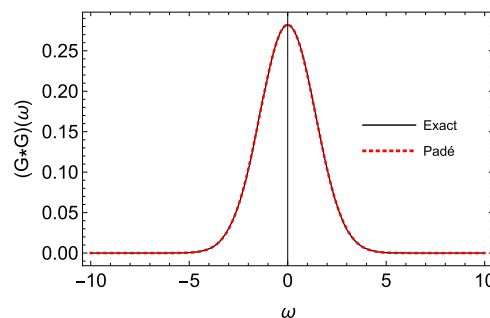

FIG. 2. Autoconvolution function $(G_\sigma * G_\sigma)(\omega)$ for $\sigma = 1$ (black solid line) and Padé-approximation (red dashed line).

$\omega \in [-50, 50]$. The calculations have been performed with the Wolfram Mathematica package.[19]

C. Model for resolution-broadened QENS spectra

Combining Relations (20) and (28), the model for the analysis of the experimental QENS spectra of free and HupA-inhibited hAChE is given by

$$S_{\text{R}}^{(+)}(\omega) = EISF \times \tilde{R}(\omega) + (1 - EISF) \times \left(L_{\alpha,\tau} * \tilde{R}\right)(\omega), \quad (39)$$

where

$$L_{\alpha,\tau}(\omega) = \tau L_{\alpha}(\omega\tau) \quad (40)$$

is the scaled version of the generalized Lorentzian defined in Eq. (21). The **q**-dependent fit parameters in our model for the resolution broadened QENS spectra are thus

1. the EISF,
2. the form parameter α, and
3. the time scale parameter τ.

As in Ref. 8, the EISF is fitted together with the two parameters α and τ describing the truly quasielastic part of the spectrum, where the convolution integral $\left(L_{\alpha,\tau} * \tilde{R}\right)(\omega)$ is approximated by the method described in Sec. III B. The form and the construction of the model for the resolution function, $\tilde{R}(\omega)$, which was adjusted to corresponding vanadium spectra, are described in the Appendix.

IV. RESULTS

Figure 3 shows a lin-log plot of the raw QENS spectrum from free and HupA-inhibited hAChE at $q = 1.0$ Å^{-1} (blue and red dots, respectively), together with the corresponding instrumental resolution function from a vanadium run (orange dots).[18] We note here that the experimental data have been recorded on the IN6 spectrometer at the Institut Laue-Langevin in Grenoble.[20] The figure shows that systematic differences between the experimental QENS spectra of HupA-inhibited and free hAChE are hardly visible.

The capability of our model to account for subtle changes in QENS spectra is demonstrated in Fig. 4. In the upper panel, we compare the QENS spectrum of free hAChE with the corresponding fit (blue dots and magenta solid line), and in the lower panel, the difference between the QENS spectra of inhibited and free hAChE (hAChE + HupA − hAChE) with the corresponding difference of the model fits (gray and magenta solid lines, respectively). The HupA-induced intensity changes are in the subpercent region, but they are systematic since the decrease of the elastic line leads to a small increase of the intensity in the adjacent quasielastic domain, which is imposed by the sum rule $\int_{-\infty}^{+\infty} d\omega\, S(\mathbf{q}, \omega) = 1$. It is remarkable that the corresponding difference plot for the resolution-broadened model dynamic structure factors (magenta solid line) reproduces the experimental data quite well, which indicates that the fits are sensitive to very small systematic changes in the QENS spectra.

The fitted EISFs displayed in Fig. 5 show that the elastic component for HupA-inhibited hAChE is slightly smaller than that for
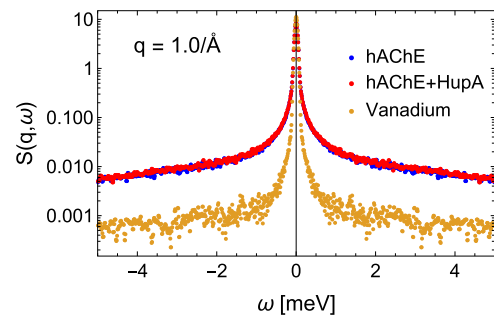

FIG. 3. Experimental QENS spectra (lin-log plot) for the free hAChE (blue), HupA-inhibited hAChE (red), and vanadium for $q = 1.0$ Å^{-1} (orange).[18] Here, ω is defined to be an energy transfer.

free hAChE, i.e., the average motional amplitudes of the hydrogen atoms in HupA-inhibited hAChE are slightly enhanced. This is also expressed by the central line in the difference data presented in Fig. 4, and we note here that the figures are similar for all q-values (not shown here).

Figure 6 shows that both the form and time scale parameters, α and τ, respectively, decay with increasing q. This expresses that relaxation processes for increasingly localized motions are faster and have less exponential characteristics. The decrease of τ with
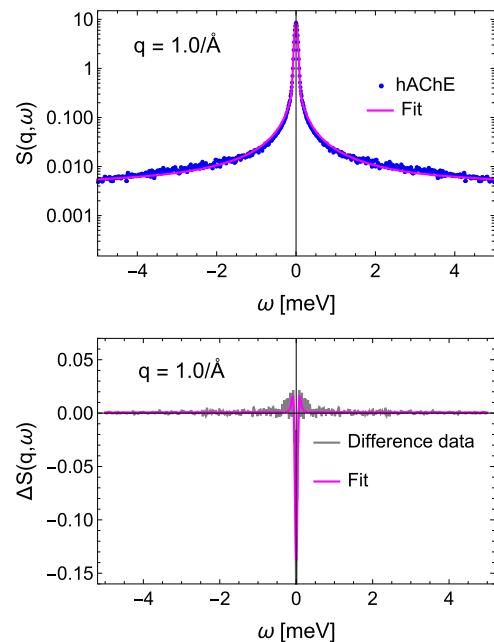

FIG. 4. Upper panel: QENS spectrum (lin-log plot) for pure hAChE at $q = 1.0$ Å^{-1} (blue dots) and fitted model (solid magenta line). Lower panel: Difference between the experimental QENS spectra of HupA-inhibited and free hAChE for $q = 1.0$ Å^{-1} (solid gray line) and the corresponding difference of the fitted models (magenta solid line). In both panels, ω is defined to be an energy transfer.
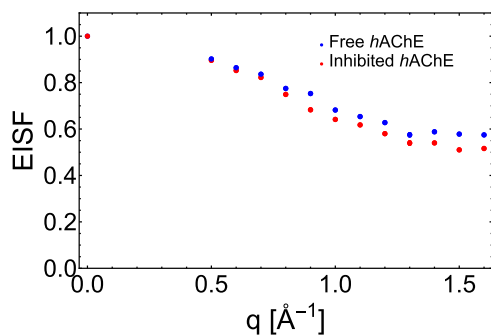
FIG. 5. EISF obtained from the fit of Expression (39) for free and HupA-inhibited hAChE (blue and red dots, respectively). The error bars are too small to be visible.

FIG. 7. Model energy barrier spectrum $P(\epsilon)$ as a function of q for free and inhibited hAChE (bluish and reddish surfaces, respectively).

q is here, however, very small, in contrast to our findings in the precedent study,[8] where τ decreased more clearly than α. The problem is the strong interdependence of the fit parameters α and τ and that we work here with instrument convolved data, which mask the detailed structure of the true quasielastic spectrum. Independent of q, the effect of inhibition through HupA on the internal dynamics of hAChE can be resumed by a slight increase of the relaxation time scale τ and an enhanced nonexponential characteristic, which is expressed by a decrease of the form parameter α.
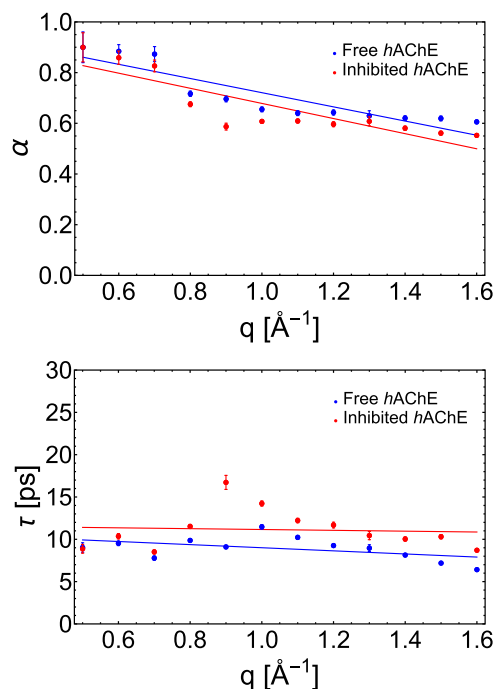

FIG. 6. The q-decay of the fitted parameters α and τ for the free and the HupA-inhibited hAChE (blue and red, respectively). Points correspond to fitted parameters and solid lines to linear fits. Error bars can be partially seen.
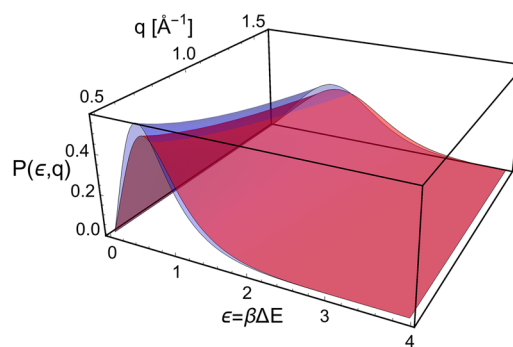
The distribution of energy barriers given in Fig. 7 shows that the effect of lowering α leads to a larger dispersion and a slight shift to higher barriers, which are consistent with the increase of the relaxation time scale, τ.

The results for all parameters of the model spectra and, in particular, their changes upon binding of HupA are consistent with those found in our previous work.[8] We note in this context that our results for the EISF confirm observations by Peters *et al.* on the same system[21] and by Balog *et al.*,[6] who have found by normal mode analysis and MD simulation that binding of the cancer drug methotrexate softens the potential and enhances the motional amplitudes of its target protein, dihydrofolate reductase. The latter point might appear counter-intuitive, in the sense that ligand binding is intuitively expected to stiffen a protein. This has been, in fact, observed for some covalently bound ligands (see Ref. 22 and references herein). The increase of the atomic motional amplitudes that we observe could be attributed to the fact that HupA is *reversibly* bound to hAChE. Since the entering and leaving of HupA ligands lead to nonnegligible conformational changes of hAChE and since the binding kinetics operates on time scales which are much longer than those accessible to QENS, the neutrons see effectively a superposition of more or less perturbed molecular structures between free and inhibited hAChE. In the experimental data, the configurational transition between the potential wells corresponding, respectively, to free and inhibited hAChE appears then as a motion in a single effective potential well, which is broader than the individual ones, and to apparently increased motional amplitudes.

We also mention that the standard deviations of the fitted parameters have been plotted as error bars, which are, however, hardly visible in the plots. What count, however, mostly here are the clearly visible systematic changes of the fitted parameters and their global variation with q.

V. RÉSUMÉ

The aim of this paper was to consolidate our previous analysis[8] of QENS spectra from free and Huperzine A-inhibited human acetylcholinesterase by a direct analysis of the resolution-broadened QENS spectra in the frequency space. The analysis in Ref. 8
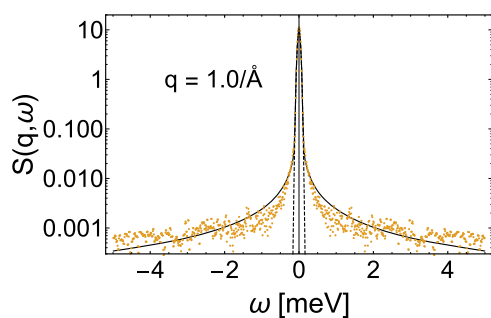
FIG. 8. Lin-log plot of the experimental instrumental resolution function from a vanadium run for $q = 1.0$ Å^{-1} (orange points) together with the fitted model (A1) (solid black line) and the fitted normalized Gaussian function (dashed black line). Here, ω is defined to be an energy transfer.

was performed by fitting a "minimal" three-parameter model to the resolution-deconvolved intermediate scattering function, which involves a numerical Fourier transform of the experimental QENS spectra. The corresponding unavoidable aliasing errors are difficult to estimate and do not occur in the direct analysis of QENS spectra in the frequency space. The latter approach necessitates, however, an analytical "fittable" model for the resolution-broadened experimental QENS spectra as well as a good model for the instrumental resolution function. Both challenges were met by using a Padé approximant for the Laplace transformed instrumental time window, which was chosen to be the product of a Gaussian window and a slowly decaying stretched Mittag-Leffler function. In frequency space, the resulting model for the instrumental resolution function is a generalization of the well-known Voigt function.[13] We note here that the representation of the instrumental resolution function by the dominating Gaussian profile alone is not sufficient for detecting subtle changes in the observed QENS spectra of hAChE upon inhibition through HupA (see Fig. 8 in the Appendix).

We have demonstrated that our model is able to extract information from extremely small but nevertheless significant changes in the QENS spectra which are in the (sub)percent region. These changes are remarkably well reproduced and confirm the results of our previous work.[8] A technical key point in our study was the use of symbolic and numerical calculations with the Wolfram Mathematica package.[19] We finally remark that the direct analysis method for QENS spectra presented here, as well as the analysis in the time domain used in Ref. 8, is suitable for QENS studies of biomolecular and complex molecular systems in general. They can be expected to be particularly useful to reveal very small changes in the dynamics upon external stress in a broader sense, such as hydrostatic pressure, temperature, solvent changes, etc.

APPENDIX: MODEL FOR THE INSTRUMENTAL RESOLUTION

In the following, we describe the model for the instrumental resolution of the IN6 spectrometer of the Institut Laue-Langevin in Grenoble on which the QENS experiments were performed. The experimental basis for the instrumental resolution are vanadium spectra, which have been recorded at room temperature. At a first glance, these spectra can be well represented by Gaussian functions, but the lin-log plot in Fig. 8 shows that this is not the case and, in particular, that the wings are missing.

To account for these wings, we describe the resolution function $\tilde{R}(\omega)$ by the convolution of a normalized Gaussian function with a scaled form of the generalized Lorentzian (21). Replacing $\alpha \rightarrow \alpha_R$ and $\tau \rightarrow \tau_R$ for clarity, we have

$$\tilde{R}(\omega) = \left(L_{\alpha_R, \tau_R} * G_\sigma\right)(\omega), \tag{A1}$$

where

$$G_\sigma(\omega) = \frac{e^{-\frac{\omega^2}{2\sigma^2}}}{\sqrt{2\pi}\sigma} \tag{A2}$$

is a normalized Gaussian function of width σ and

$$L_{\alpha_R, \tau_R}(\omega) = \tau_R L_{\alpha_R}(\omega\tau_R). \tag{A3}$$

We note that Expression (A1) becomes the well-known Voigt profile[13] for the special case $\alpha_R = 1$.

The convolution (A1) was performed with the semianalytical method described in Sec. III B of the main text, using a Padé-approximation for the Laplace-transformed Gaussian function $\hat{G}_\sigma(s)$. Concerning the parameters, we note that $\tau_R \approx 1.5 \times 10^7$ ps and $\alpha_R \approx 0.2$ for all q-values. The fits are not as good as those for the QENS data, but clearly much better than those with a Gaussian function alone.

In order to account for the strong dominance of the Gaussian component in the vanadium spectra as well as for the strong interdependence of the fit parameters $\{\sigma, \alpha_R, \tau_R\}$, we performed the fit of Expression (A1) in two steps. In a first step, we fixed σ by a fit of Expression (A2) and used the result to fit, in a second step, Expression (A1) to adjust the remaining parameters α_R and τ_R. The orders of polynomials $P(s)$ and $Q(s)$ in the Padé approximation of $\hat{G}_\sigma(s)$ were set to $m = n = 8$, and the reference point was chosen to be the σ-value found from the fit of the Gaussian function, $s_0 = \sigma$. Figure 8 displays the fit of the vanadium spectrum for $q = 1$ Å^{-1}. The σ parameter was found to be 0.036 meV, which is consistent with the instrumental resolution of 70 μeV $\approx$ FWHM for the incident neutron wave length of 5.12 Å that was used to record the QENS spectra.

REFERENCES

[1]T. Springer, *Springer Tracts in Modern Physics* (Springer Berlin Heidelberg, Berlin, Heidelberg, 1972), Vol. 64, pp. 1–100, ISBN: 978-3-540-05808-3; 978-3-540-37457-2.

[2]M. Bée, *Quasielastic Neutron Scattering: Principles and Applications in Solid State Chemistry, Biology and Materials Science* (Adam Hilger, Bristol, 1988).

[3]J. C. Smith, P. Tan, L. Petridis, and L. Hong, Annu. Rev. Biophys. **47**, 335 (2018).

[4] R. Ashkar, H. Z. Bilheux, H. Bordallo, R. Briber, D. J. E. Callaway, X. Cheng, X.-Q. Chu, J. E. Curtis, M. Dadmun, P. Fenimore *et al.*, Acta Crystallogr., Sect. D: Struct. Biol. **74**, 1129 (2018).

[5] V. Calandrini, V. Hamon, K. Hinsen, P. Calligari, M. C. Bellissent-Funel, and G. R. Kneller, Chem. Phys. **345**, 289 (2008).

[6] E. Balog, D. Perahia, J. C. Smith, and F. Merzel, J. Phys. Chem. **115**, 6811 (2011).

[7] G. R. Kneller, Proc. Natl. Acad. Sci. U. S. A. **115**, 9450 (2018).

[8] M. Saouessi, J. Peters, and G. R. Kneller, J. Chem. Phys. **150**, 161104 (2019).

[9] R. Zwanzig, Proc. Natl. Acad. Sci. U. S. A. **85**, 2029 (1988).

[10] H. Frauenfelder, S. G. Sligar, and P. G. Wolynes, Science **254**, 1598 (1991).

[11] P. Schofield, Phys. Rev. Lett. **4**, 239 (1960).

[12] R. Hilfer and H. J. Seybold, Integr. Transforms Spec. Funct. **17**, 637 (2006).

[13] *NIST Handbook of Mathematical Functions*, edited by F. W. J. Olver, D. W. Lozier, R. F. Boisvert, and C. W. Clark (Cambridge University Press, 2010).

[14] P. Cheridito, H. Kawaguchi, and M. Maejima, Electron. J. Probab. **8**, 14 (2003).

[15] G. Uhlenbeck and L. Ornstein, Phys. Rev. **36**, 823 (1930).

[16] R. Metzler, E. Barkai, and J. Klafter, Phys. Rev. Lett. **82**, 3563 (1999).

[17] G. R. Kneller, Phys. Chem. Chem. Phys. **7**, 2641 (2005).

[18] M. Trapp, M. Tehei, M. Trovaslet, F. Nachon, N. Martinez, M. M. Koza, M. Weik, P. Masson, and J. Peters, J. R. Soc. Interface **11**, 20140372 (2014).

[19] Wolfram Research, Inc., Mathematica, Version 11.1, Wolfram Research, Inc., Champaign, IL, USA, 2017.

[20] See https://www.ill.eu/instruments-support/instruments-groups/instruments/in6-sharp/ for IN6-Sharp - Cold Neutron Time-Focussing Time-of-Flight Spectrometer.

[21] J. Peters, N. Martinez, M. Trovaslet, K. Scannapieco, M. M. Koza, P. Masson, and F. Nachon, Phys. Chem. Chem. Phys. **18**, 12992 (2016).

[22] C. D. Andersson, N. Martinez, D. Zeller, A. Allgardsson, M. M. Koza, B. Frick, F. Ekström, J. Peters, and A. Linusson, J. Phys. Chem. **122**, 8516 (2018).